

A Method to Retrieve the Reflectivity Signature at $3.75 \mu\text{m}$ from AVHRR Data

J. C. Roger* and E. F. Vermote*

Global monitoring of land surface properties has primarily relied on the AVHRR red and near-infrared channels through use of the NDVI. The AVHRR Channel 3, centered at $3.75 \mu\text{m}$, has been shown to be sensitive to vegetation on a local scale. A method to separate the reflected and emitted components in this channel has been developed. The $3.75\text{-}\mu\text{m}$ reflectivity is computed by subtracting the thermal contribution from the total signal and dividing the remaining signal component by atmospheric transmission and solar irradiance. The thermal contribution is estimated by using thermal infrared Channels 4 and 5 as well as NDVI to estimate infrared surface emissivities. The atmospheric transmission is computed with MODTRAN2 and uses integrated water vapor derived from the Split Window Technique. The formula derived are validated over ocean using sun glint observations and land using the FIFE-87 data set. Despite the uncertainties inherent to the procedure we adopted, quantitative use of the derived reflectance at $3.75 \mu\text{m}$ appears possible. Published by Elsevier Science Inc., 1998

INTRODUCTION

For the last 15 years, data of the Earth-atmosphere system have been continuously acquired from the Advanced Very High Resolution Radiometers (AVHRRs) onboard NOAA polar orbiting satellites. The AVHRR carries visible, infrared, and thermal bands, and provides a complete coverage of the Earth twice a day from each of the two platforms (morning and afternoon pass). These data are a valuable source of information for monitoring ocean, terrestrial, and atmospheric processes at local and global scales.

Over ocean, Channels 4 and 5 have been routinely used to estimate sea surface temperature (Prabhakara et al., 1974; McMillin, 1975), and Channel 1 to estimate aerosol optical thickness (Rao et al., 1989). Over land, AVHRR Channels 1 and 2, the red and near-infrared spectral bands, are used to derive the normalized difference vegetation index (NDVI) (Tucker et al., 1981; Justice et al., 1985) and to estimate the biomass production (Daughtry et al., 1983; Tucker et al., 1983; 1985). Channel 3 has been used qualitatively to assess deforestation (Malingreau et al., 1989) and biomass burning (Setzer and Pereira, 1991), or to detect fires (Dozier, 1981; Matson and Dozier, 1981).

Recent advances in modeling Channels 4 and 5 signals over land (Becker and Li, 1990; Kerr et al., 1992; Otlé and Vidal-Madjar, 1992; Seguin et al., 1992) makes it possible to use Channels 4, 5, and 3 to derive a quantitative estimate of the reflectance at $3.75 \mu\text{m}$. The use of the derived mid-infrared reflectance is important for AVHRR aerosol retrieval method over land (Vermote et al., 1992; 1994), but could also be of use for other applications because of the addition of a reflectance band.

In this article, we derive a formula to estimate reflectance at $3.75 \mu\text{m}$ based on Channels 3, 4, 5, NDVI data, and MODTRAN2 (Berk et al., 1989) simulations (next section). The method consists of estimating the part of the signal in Channel 3 due to emitted radiation (thermal component) and subtracting it from the total signal to deduce the reflective component. The thermal component in Channel 3 is expressed as a second-degree polynomial of the observed signals from Channels 4 and 5 and emissivities in 4 and 5. Over sea, emissivities in Channels 3, 4, and 5 are known (Takashima and Takayama, 1981; Masuda et al., 1988). Over land, the emissivities in Channels 4 and 5 are assumed to be equal to a linear function of the logarithm of NDVI (Van de Griend and Owe, 1993). The computation of the reflectivity requires the upward and downward atmospheric transmission. This in turn requires integrated water vapor con-

*Department of Geography, University of Maryland, College Park
Address correspondence to E. F. Vermote, NASA/GSFC/Code 923, Greenbelt, MD 20771.

Received 12 February 1996; revised 3 April 1997.

tent. The water vapor is retrieved directly from Channels 4 and 5 using the split window technique. The accuracy of water vapor retrieval of ocean is examined using one year of SSM/I water vapor data over the Pacific Ocean.

The derived reflectivity is examined in the third section. We first validate the formula in the case of sunglint observations where the emissivities of Channels 3, 4, and 5 can be computed. Next, we examine the land case for which the emissivity in Channels 4 and 5 has to be deduced from NDVI. We apply our technique and compare the retrieved thermal component at $3.75 \mu\text{m}$ to computations done using ground measurements performed during the FIFE-87 experiment.

DERIVATION OF SURFACE REFLECTANCE IN AVHRR CHANNEL 3

Theoretical Background

In this section, we assume that the effect of aerosols in the thermal range (Channels 3, 4, and 5 of AVHRR) is negligible. The impact of aerosols will be treated in the error budget.

For a cloud-free atmosphere under local thermodynamic equilibrium, the measured radiance R_i^m emerging from the top of the atmosphere and recorded in thermal channels i (3, 4, or 5 for AVHRR) at a view zenith angle θ_v and view azimuth φ_v with a Sun at coordinates (θ_s, φ_s) is given by [following Becker and Li (1990) notations]

$$R_i^m(\theta_s, \theta_v, \varphi_s, \varphi_v) = \int f_i(\lambda) \varepsilon_i(\theta_s, \varphi_s) B_\lambda(T_s) \tau_\lambda(\theta_s, \varphi_s) d\lambda \\ + \iint f_i(\lambda) B_\lambda(T_p) \frac{\delta\tau_\lambda(\theta_v, \varphi_v, p)}{\delta p} dp d\lambda \\ + \int f_i(\lambda) \left[\rho_{b\lambda}(\theta_v, \varphi_v, \theta', \varphi') L_{s\lambda}(\theta', \varphi') \tau_\lambda(\theta_s, \varphi_s) \right. \\ \left. \times \cos(\theta') \sin(\theta') d\theta' d\varphi' d\lambda \right] \quad (1)$$

with

$$L_{s\lambda}(\theta', \varphi') = \int B_\lambda(T_p) \frac{\delta\tau_\lambda'(\theta', p)}{\delta p} dp + \delta(\varphi_s - \varphi') \delta(\theta_s - \theta') \\ \times \frac{\cos(\theta_s) E_\lambda^s}{\pi} \tau_\lambda'(\theta_s), \quad (2)$$

where $f_i(\lambda)$ is the spectral response of the radiometer in channel i , ε_i is the surface spectral emissivity, $B_\lambda(T)$ is the Planck spectral radiance function for a temperature T , T_s is the surface temperature, τ_λ (resp. τ_λ') is the upward (resp. downward) spectral transmittance of the atmosphere, $\rho_{b\lambda}$ is the spectral bidirectional reflectivity of the surface, p is the pressure, and E_λ^s is the spectral exo-atmospheric irradiance.

The first term of Eq. (1) is related to the surface contribution, the second term to the atmospheric contribution along the upward path, and the third term to the atmospheric contribution along the downward path that reaches the surface $L_{s\lambda}$, reflected according to $\rho_{b\lambda}$ and transmitted upward through the atmosphere by τ_λ . For the source term $L_{s\lambda}$ we distinguish between the atmo-

spheric thermal radiation part [first part of Eq. (2)], and the solar part [second part of Eq. (2)].

We call "reflective contribution" (we will use in the following the superscript r) the reflection of the solar part by the surface and transmitted to the top of that atmosphere, that is,

$$R_i^r(\theta_s, \theta_v, \varphi_s, \varphi_v) = \frac{\tau_\lambda'(\theta_s) \rho_{b\lambda}(\theta_s, \theta_v, \varphi_s, \varphi_v) \tau_\lambda(\theta_v) E_\lambda^s \cos(\theta_s)}{\pi}, \quad (3)$$

and "emissive (or thermal) contribution" (superscript e) the part due to the thermal infrared contribution, that is,

$$R_i^e(\theta_s, \varphi_v) = \varepsilon_i(\theta_s, \varphi_v) B_3(T_s) \tau_3(\theta_v) + \int B_3(T_p) \frac{\delta\tau_3(\theta_v, p)}{\delta p} dp \\ + \left[\int \rho_3(\theta_s, \varphi_s, \theta', \varphi') B_3(T_p) \frac{\delta\tau_3'(\theta', p)}{\delta p} dp \tau_3(\theta_s, \varphi_s) \right. \\ \left. \times \sin(\theta') \cos(\theta') d\theta' \right]. \quad (4)$$

Thus, in a simplified manner, we write $R_i^m = R_i^e + R_i^r$. Nevertheless, the rapid decrease of the solar irradiance with wavelength in the infrared allows us to assume no solar reflective contribution in Channels 4 and 5 and therefore write the following set of equations for Channels 3, 4, and 5 corresponding to what can be measured at the top of the atmosphere:

$$R_3^m(\theta_s, \theta_v, \varphi_s, \varphi_v) = R_3^e(\theta_s, \varphi_v) + R_3^r(\theta_s, \theta_v, \varphi_s, \varphi_v), \\ R_4^m(\theta_s, \varphi_v) = R_4^e(\theta_s, \varphi_v), \\ R_5^m(\theta_s, \varphi_v) = R_5^e(\theta_s, \varphi_v). \quad (5)$$

In practice, for each channel i ($i=3,4,5$) the AVHRR radiances, R_i^m and the thermal radiances R_i^e are converted from brightness temperature values T_i^m and T_i^e using the Planck function B_i and the wavelength λ_i given in Table 1 by NOAA (Kidwell, 1991); then the Eqs. (5) become

$$B_3(T_3^m(\theta_s, \theta_v, \varphi_s, \varphi_v)) = B_3(T_3^e(\theta_s, \varphi_v)) + R_3^r(\theta_s, \theta_v, \varphi_s, \varphi_v), \\ B_4(T_4^m(\theta_s, \varphi_v)) = B_4(T_4^e(\theta_s, \varphi_v)), \\ B_5(T_5^m(\theta_s, \varphi_v)) = B_5(T_5^e(\theta_s, \varphi_v)), \quad (6)$$

and the "reflective contribution" in Channel 3 is expressed by

$$R_3^r(\theta_s, \theta_v, \varphi_s, \varphi_v) = B_3(T_3^m(\theta_s, \theta_v, \varphi_s, \varphi_v)) - B_3(T_3^e(\theta_s, \varphi_v)). \quad (7)$$

Computation of the Reflectance over Sea

Over clear ocean (no aerosol, no cloud) the emissivities in Channels 3, 4, and 5 are modeled as a function of the agitation state of the surface (Masuda et al., 1988; Takashima and Takayama, 1981). The surface reflectance $\rho_3(\theta_s, \theta_v, \varphi_s, \varphi_v)$ is directly expressed by

$$\rho_3(\theta_s, \theta_v, \varphi_s, \varphi_v) = \frac{\pi \{ B_3(T_3^m(\theta_s, \theta_v, \varphi_s, \varphi_v)) - B_3(T_3^e(\theta_s, \varphi_v)) \}}{E_3^s \cos(\theta_s) \tau_3(\theta_s) \tau_3(\theta_v)}, \quad (8)$$

where the $T_3^e(\theta_v)$ computation depends on emissivity in Channel 3 and is computed as a function of the temperature observed in Channels 4 and 5 and emissivities (see the subsection after next). Table 1 lists the emissivities used in Channels 3, 4, and 5 solely as a function of view angle because the variation with wind speed is small.

Table 1. Emissivities of the Sea Waters Used for the Computations in Channels 3, 4, and 5 (Given versus the Viewing Angle θ_v) (from Masuda et al., 1988)

	0°	10°	20°	30°	40°	50°	60°	70°
Channel 3	0.974	0.974	0.974	0.972	0.967	0.955	0.925	0.857
Channel 4	0.992	0.992	0.992	0.991	0.989	0.981	0.958	0.903
Channel 5	0.988	0.988	0.988	0.986	0.983	0.972	0.942	0.875

Computation of the Reflectance over Land

Over land the problem is more complex because emissivities in Channels 3, 4, and 5 are unknown and vary with cover type (Salisbury and D'Aria, 1992; Van de Griend and Owe, 1993). To solve the system, we make several assumptions.

First, if we assume that the surface is a Lambertian reflector and using the Kirchoff relation applied to Channel 3, $\rho_3=1-\varepsilon_3$, the "thermal" radiance in Channel 3 becomes

$$R_3^c(\theta_v) = B_3(T_s)\tau_3(\theta_v) + \int B_3(T_p) \frac{\delta\tau_3(\theta_v, p)}{\delta p} dp - \rho_3 B_3(T_s)\tau_3(\theta_v) + \rho_3 \tau_3(\theta_v) \iint B_3(T_p) \frac{\delta\tau_3(\theta', p)}{\delta p} dp \sin(\theta') \cos(\theta') d\theta'. \quad (9)$$

In an advanced approach the non-Lambertian behavior of the surface may be introduced using a form factor $F(\theta_v, \varphi_v)$ as described by Becker et al. (1986) and Nerry et al. (1988).

Let us now define the thermal radiance for an emissivity $\varepsilon_3=1$:

$$R_3^c(\theta_v, \varepsilon_3=1) = B_3(T_s^*(\theta_v, \varepsilon_3=1)) = B_3(T_s)\tau_3(\theta_v) + \int B_3(T_p) \frac{\delta\tau_3(\theta_v, p)}{\delta p} dp. \quad (10)$$

We can notice that the two first terms of the Eq. (9) correspond to the radiance for an emissivity $\varepsilon_3=1$ given Eq. (10). Then, if we substitute Eq. (10) into Eq. (11), the radiance in Channel 3 can be written

$$R_3^c(\theta_v, \varepsilon_3) = R_3^c(\theta_v, \varepsilon_3=1) + \rho_3 \{-B_3(T_s)\tau_3(\theta_v) + \iint B_3(T_p) \frac{\delta\tau_3(\theta', p)}{\delta p} dp \tau_3(\theta_v) \sin(2\theta') d\theta'\}. \quad (11)$$

Equation (11) shows that the thermal radiance can be split into two parts. The first part corresponds to the emitted radiance for a surface emissivity equal to 1. The second part is related to the effect of the surface reflectance. Since the radiance emitted from the ground when $\varepsilon_3=1$ represents the major part of the radiance observed at the top of the atmosphere (about 80%), we write

$$B_3(T_s)\tau_3(\theta_v) \approx \beta \cdot R_3^c(\theta_v, \varepsilon_3=1), \quad (12)$$

where β is principally a function of $\tau_3(\theta_v)$.

Likewise we assume that the downwelling atmospheric radiance is related to atmospheric emissive processes and write

$$\iint B_3(T_p) \frac{\delta\tau_3(\theta', p)}{\delta p} dp \tau_3(\theta_v) \sin(2\theta') d\theta' \approx a \cdot R_3^c(\theta_v, \varepsilon_3=1), \quad (13)$$

where a is principally a function of $\tau_3(\theta_v)$.

By introducing the function $\gamma = \beta - a$ (with $\beta > a$), we rewrite Eq. (10) as

$$R_3^c(\theta_v, \varepsilon_3) = R_3^c(\theta_v, \varepsilon_3=1)[1 - \gamma \cdot \rho_3] \quad (14a)$$

or

$$B_3(T_s^*(\theta_v, \varepsilon_3)) = B_3(T_s^*(\theta_v, \varepsilon_3=1))[1 - \gamma \cdot \rho_3], \quad (14b)$$

where γ is a function of $\tau_3(\theta_v)$. Thus, the reflectivity signature is considered as a perturbation of the TOA signal one should observe if the emissivity was equal to 1, with γ a parameter depending on the atmosphere. From a data set produced by MODTRAN2 runs (36 different atmospheres with a water vapor varying from 0 to 6.5 g/cm², view zenith angle from 0° to 60°) we find

$$\gamma \approx \tau_3(\theta_v). \quad (15)$$

The comparison between $R_3^c(\theta_v, \varepsilon_3)$ and $R_3^c(\theta_v, \varepsilon_3=1) \cdot [1 - \tau_3(\theta_v) \cdot \rho_3]$ is shown in Figure 1. The agreement between the two plots is very good (1% RMS).

Finally, introducing Eqs. (14) and (15) into Eq. (8), the surface reflectance ρ_3 can be computed using the formula

Figure 1. Comparison between $R_3^c(\theta_v, \varepsilon_3)$ and $R_3^c(\theta_v, \varepsilon_3=1) \cdot [1 - \tau_3(\theta_v) \cdot \rho_3]$ for land simulations.

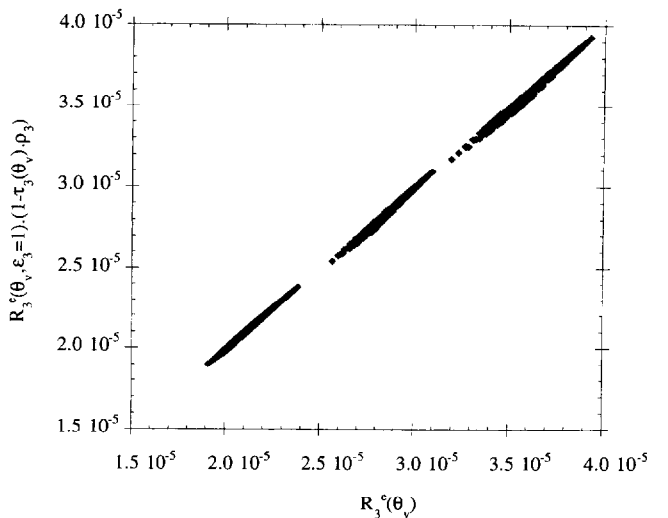


Table 2. Wavelengths (in μm) Used for the Planck's Function B^a

	Channel 3	Channel 4	Channel 5	E_3 [$\text{W m}^{-2} (\text{cm}^{-1})^{-1}$]
NOAA 9	3.734	10.759	11.892	16.68
NOAA 11	3.744	10.779	11.928	16.68

^a Also reported is the exoatmospheric irradiance.

$$\rho_3 = \frac{\pi\{R_3^u(\theta_s, \theta_t) - R_3^u(\theta_s, \varepsilon_3=1)\}}{\cos(\theta_s)E_3\tau_3(\theta_s)\tau_3(\theta_t) - \pi R_3^u(\theta_s, \varepsilon_3=1)\tau_3(\theta_t)}, \quad (16)$$

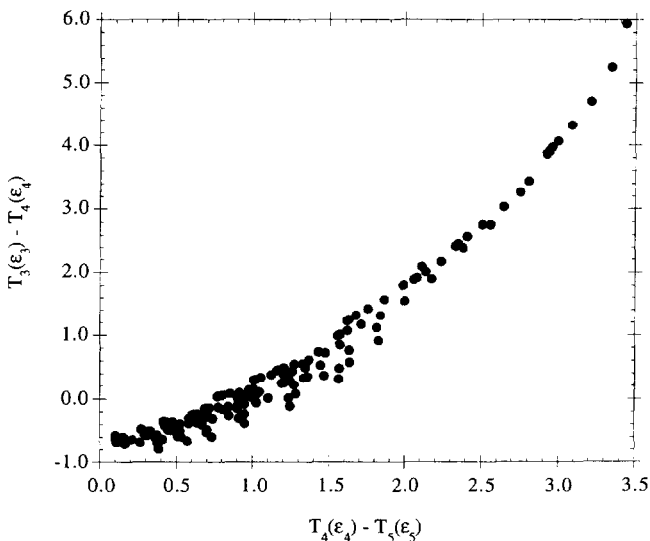
where E_3 is given in Table 2 and with $R_3^u = B_3(T_3)$. We tested this formula with theoretical computations from MODTRAN2, and the comparison between ρ_3 computed by Eq. (16) and ρ_3 entered as an input of the simulation shows an accuracy ranging from 0.5% RMS for $\theta_s=0^\circ$ to 3.5% RMS for $\theta_s=60^\circ$.

Computation of T_3^v

The estimation of the thermal component in Channel 3 is based on the relationship that exists between this component and the signal observed in Channels 4 and 5. This component depends, as shown in Eq. (1), on the surface temperature, the atmospheric profile (temperature, pressure, and relative humidity) and on the emissivity in Channel 3: more unknowns than equations. Therefore, we used MODTRAN2 to generate a data set of (T_3^v , T_4^v , T_5^v) values for our set of atmospheric profiles as well as surface emissivities (Lambertian case, from 1.00 to 0.80) and zenith angles (up to 60°). Using this database, we can define empirical relationships between $T_3^v(\varepsilon_3) - T_4^v(\varepsilon_4)$ and $T_4^v(\varepsilon_4) - T_5^v(\varepsilon_5)$.

Over oceans, emissivities in Channels 3, 4, and 5 are fixed (see Table 1). Then, the relationship between

Figure 2. Comparison between $T_3^v(\varepsilon_3=1) - T_4^v$ versus $T_4^v - T_5^v$ using MODTRAN2 simulations in the case of ocean views with θ_s ranging from 0° to 60° .



$T_3^v - T_4^v$ and $T_4^v - T_5^v$ can be directly plotted. Figure 2 shows that for zenith angles ranging from 0° to 60° , $T_3^v - T_4^v$ can be expressed as a second-order polynomial in $T_4^v - T_5^v$. Then the "emissive" temperature can be written as

$$T_3^v = T_4^v + n_0 + n_1(T_4^v - T_5^v) + n_2(T_4^v - T_5^v)^2 \quad (17)$$

with $T_4^v = T_4^u$ and $T_5^v = T_5^u$ and where n_i are given for NOAA 9 and NOAA 11 (Table 3).

Emissivities in Channels 4 and 5 over land surfaces may be quite different from unity and may vary spatially and temporally. For the time being, we assume over land no spectral differences between the emissivity in these channels, and we shall call it ε_{45} . Following Van de Griend and Owe (1993), the emissivity in the infrared channels is a function of surface greenness, NDVI. We compute NDVI from AVHRR Channels 1 and 2 and get ε_{45} using their formula, which is

$$\varepsilon_{45} = 1.009 + 0.047 \cdot \ln(\text{NDVI}). \quad (18)$$

We show in Figure 3 $T_3^v(\varepsilon_3=1) - T_4^v$ versus $T_4^v - T_5^v$ for $\varepsilon_{45}=0.94$ and $\varepsilon_{45}=0.97$. The relationship is still a second-order polynomial with coefficients depending on ε_{45} (see Fig. 4). By performing a second-order polynomial regression of the polynomial coefficients, we finally obtain for data acquired at sea level

$$T_3^v(\varepsilon_3=1) = T_4^v + m_0 + m_1 \cdot (T_4^v - T_5^v) + m_2 \cdot (T_4^v - T_5^v)^2 \quad (19)$$

with $T_4^v = T_4^u$ and $T_5^v = T_5^u$ and where coefficients m_i are functions of ε_{45}

$$\begin{aligned} m_0 &= m_{01} + m_{02}\varepsilon_{45} + m_{03}\varepsilon_{45}^2, \\ m_1 &= m_{11} + m_{12}\varepsilon_{45} + m_{13}\varepsilon_{45}^2, \\ m_2 &= m_{21} + m_{22}\varepsilon_{45} + m_{23}\varepsilon_{45}^2, \end{aligned} \quad (20)$$

where m_{ij} are given for NOAA 9 and NOAA 11 in Table 4.

Computation of Transmission $\tau(\theta)$ in Channel 3

This gaseous transmittance in Channel 3 can be split into two parts. The first part is the water vapor transmittance and the second part includes all other atmospheric components which only depend of the solar and viewing zenith angles θ_s and θ_t .

Table 3. Coefficients n_i Used in Eq. (19) for NOAA 9 and 11

	n_0	n_1	n_2
NOAA 9	-0.777	0.155	0.445
NOAA 11	-0.675	0.255	0.449

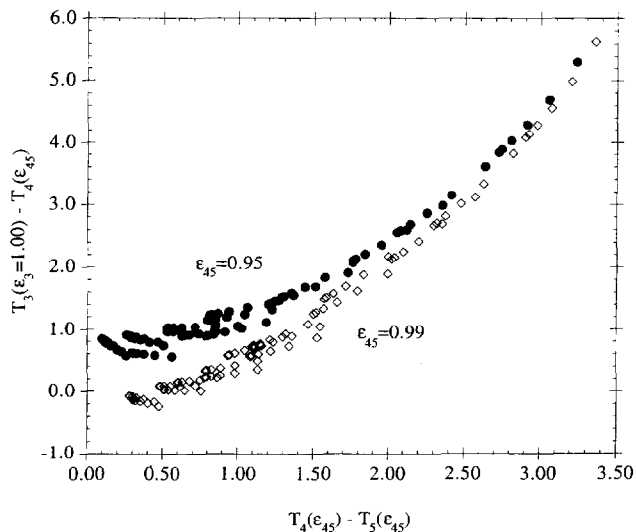


Figure 3. Comparisons between $T_3(\epsilon_3=1) - T_4$ versus $T_4 - T_5$ using MODTRAN2 simulations in the case of land views for $\epsilon_{45}=0.95$ and 0.99 .

Water Vapor Transmission

Several published studies have shown the efficiency of the split window technique (McMillin, 1971) applied to water vapor retrieval in the atmosphere (Prabhakara et al., 1974; Dalu, 1986; Schuessel, 1989; Justice, 1991; Eck and Holben, 1994). These studies report several formulations of the water vapor retrieval from $T_4 - T_5$. In the present study, we tried to improve the retrieval over ocean using our data.

For observations over ocean Dalu (1986) simulated the response of split window brightness temperature difference to water vapor assuming a linear law

$$U_{h_{20}} = A(\theta_v)(T_4^n - T_5^n), \quad (21)$$

where θ_v is the view zenith angle. We used one year of SSM/I and AVHRR data collected in time at the same location over the Pacific Ocean to test this relation. A plot of SSM/I water vapor content versus nadir measurements of $T_4^n - T_5^n$ is given Figure 5a. From this, we determine $A(0^\circ) = 1.98 \pm 0.5 \text{ g/cm}^2/\text{K}$. For a viewing angle θ_v equal to 60° , this coefficient becomes $A(60^\circ) = 1.53 \pm 0.5 \text{ g/cm}^2/\text{K}$ (Fig. 5b).

The SSM/I results were compared to theoretical computations with MODTRAN2 code. Using our 36 different atmospheres (see above), we computed the coefficient A for different angles ($0-70^\circ$). For a nadir measurements, the slope A found is very close to the SSM/I value and to Dalu's result. For the angular dependency of A , we found a law in $\cos(\theta_v)^{0.35}$, which does not follow a $\cos(\theta_v)$ law (Dalu, 1986), but which confirms the SSM/I observations (Fig. 6).

Several problems arise over land, such as the uncertainties in surface emissivity in Channels 4 and 5, the difference between skin temperature and surface air temperature. Thus, we tried to define different relationships between $T_4^n - T_5^n$ and $U_{h_{20}}$, from different data bases. For example, Roger et al. (1994) used the MAS (Modis Airborne Simulator) data and water vapor measurements from a Sun photometer to show that it is possible over the so-called dark target (emissivities close to unity) to use a similar formula than the one used for ocean views. We applied the same approach to data from the SCAR-A experiment which has been conducted in the Eastern U.S. coast on July 1993, and found (for NOAA 11)

$$U_{h_{20}} = -0.20 + 1.15(T_4^n - T_5^n)\cos(\theta_v)^{0.43}. \quad (22)$$

We derive a different relationship using the FIFE-87 data set (Sellers et al., 1992) (for NOAA 9):

$$U_{h_{20}} = 0.25 + 1.47(T_4^n - T_5^n)\cos(\theta_v)^{0.37}. \quad (23)$$

Eck and Holben (1994) reported other relationships depending on location. Therefore, we decided to define a "mean" relationship between $T_4^n - T_5^n$ and $U_{h_{20}}$. One boundary case is the dark target case; the other is the desert environment case. Then, the water vapor amount can be deduced within a mean accuracy of 0.8 g/cm^2 RMS from

$$U_{h_{20}} = 1.5(T_4^n - T_5^n)\cos(\theta_v)^{0.4}. \quad (24)$$

This "mean" formula can be useful for users who need the water vapor transmittance inside an operational procedure of computation, particularly for global study of the reflectivity at $3.75 \mu\text{m}$. It is probably better to use the water vapor amount from other sources such as the Data Assimilation Office product (Schubert et al., 1993).

To compute the water vapor transmittance, we used the theoretical data set as described above. The water

Figure 4. Polynomial coefficients for $\epsilon_3=1.00$ versus ϵ_{45} [see Eqs. (19) and (20)].

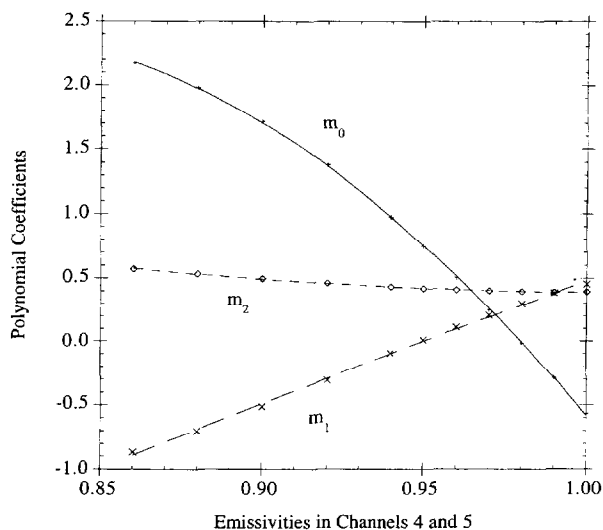


Table 4. Coefficients n_i Used in Eq. (19) for NOAA 9 and 11

	NOAA 9			NOAA 11		
	m_0	m_1	m_2	m_0	m_1	m_2
m_{11}	-47.54	-14.54	9.683	-47.30	-11.18	8.620
m_{12}	126.2	19.61	-18.22	124.0	13.87	-16.24
m_{13}	-79.33	-4.733	8.937	-77.29	-2.206	8.010

vapor transmittance can be expressed as a double exponential function of the air mass M [equal to $1/\cos(\theta_s) + 1/\cos(\theta_v)$] and of the water vapor amount U_{H_2O} , with a RMS error of about 2%,

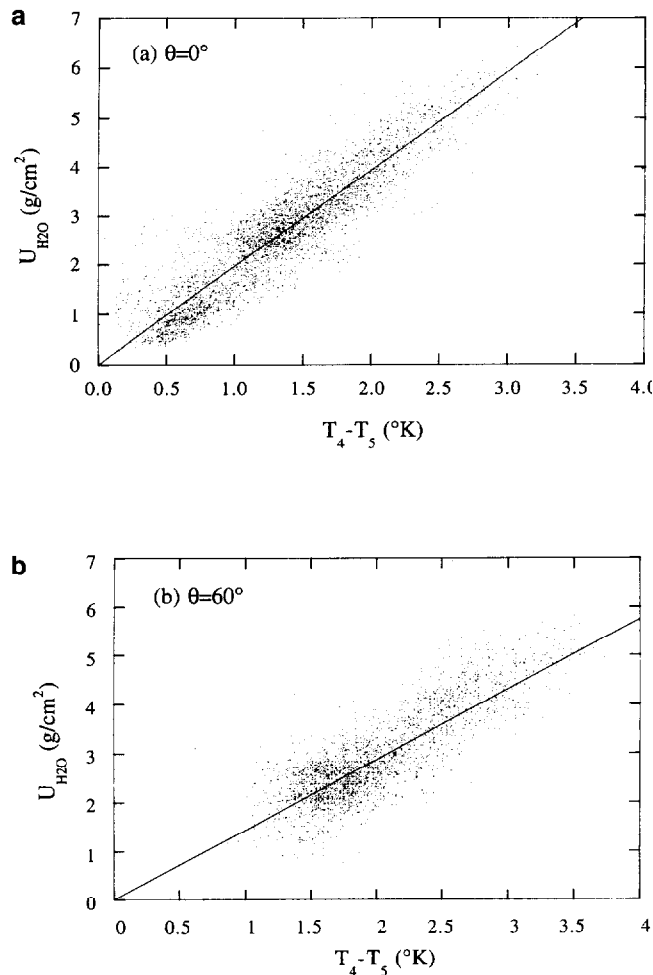
$$\tau_{3^{\text{exp}}}^{H_2O}(U_{H_2O}, \theta_s, \theta_v) = \exp(-\exp(-a + b \cdot \ln(U_{H_2O} M) + c \cdot \ln(U_{H_2O} M)^2)), \quad (25)$$

where a , b , and c are constants given in Table 5a for NOAA 9 and NOAA 11.

Transmission of the Other Gases

Except for water vapor, the atmospheric gases interacting primarily in a range of wavelengths over Channel 3 are

Figure 5. (a) Plot of U_{H_2O} from SSM/I versus $(T_4 - T_5)$ for a zenith angle equal to 0° . (b) Same as Figure 5a but for a zenith angle equal to 60° .



O_3 , H_2O , CH_4 , N_2O , N_2 , and CO_2 . Their transmittances can be assessed by a second degree polynomial function in the air mass M with a RMS error of 0.3% by

$$\tau_3^{\text{th}}(\theta_s, \theta_v) = a + b \cdot M + c \cdot M^2, \quad (26)$$

where a , b , and c are constants given in Table 5b for NOAA 9 and NOAA 11.

The total transmittance in Channel 3 is finally deduced from

$$\tau_3(\theta_s, \theta_v) = \tau_3^{\text{exp}}(U_{H_2O}, \theta_s, \theta_v) \cdot \tau_3^{\text{th}}(\theta_s, \theta_v). \quad (27)$$

Error Budget

The error $\Delta\rho_3$ in the retrieved reflectance derives from the error in the measured temperature T_3^m , the solar irradiance E_3^s , the computation of the temperature T_3 , the transmittance and the formula itself. An error budget for $\theta_s = 60^\circ$, which is a worst case, is reported in Table 6.

a. Numerical noise: The raw data are provided by NOAA. Using our processing (Vermote et al., 1994), the nonlinearity in temperature is accounted for (Weinreb, 1990). In the range for which temperatures are not saturated (for T_3^m) the error is commonly assumed to be 0.1° . We define the impact of this source by applying random errors of RMS of 0.1° to temperatures. The effect on the retrieval of ρ_3 is not negligible (about 25–30% for the lowest reflectances and about 2–4%

Figure 6. Angular dependency of $A(\theta)$ determined over sea both by the measurement and by the computations. Also reported, the law in $\cos(\theta)$.

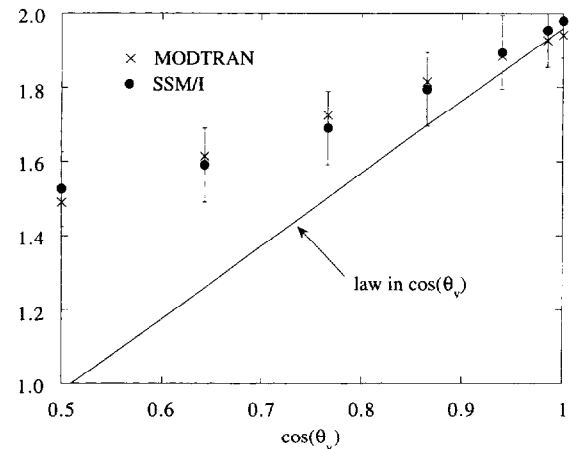


Table 6. Budget Error (RMS) on the Computation of the Reflectance in Channel 3 for a Solar Zenith Angle Equal to 60°

	$\Delta\rho/\rho(\%)$ —Sea		$\Delta\rho/\rho(\%)$ —Land	
	$\rho_3=0.02$	$\rho_3=0.20$	$\rho_3=0.02$	$\rho_3=0.20$
Numerical noise max	25	2.5	30	4
T_3 estimation	14	2	21	4
Eq. (16)	—	—	3.5	3.5
Transmittance	5	5	7.5	7.5
Sol. irradiance	30	8	10	2
Aerosol	30	8	10	2
Total (RMS)	41	10	38	10

for the highest reflectances), but it can be reduced by averaging pixels.

- b. T_3 estimation** is based on polynomial regression [Eqs. (17), (19), and (20)] and the error in its determination depends on the measured temperatures $T_4^m - T_5^m$. This regression error generates a $\Delta\rho_3/\rho_3$ of about 15% RMS for $\rho_3=0.02$ and 2% RMS for $\rho_3=0.20$ in case of land views and a $\Delta\rho_3/\rho_3$ of about 10% RMS for $\rho_3=0.02$ and 1% RMS for $\rho_3=0.20$ in case of ocean views. The uncertainty of the emissivity ε_{45} and the assumption that $\varepsilon_4=\varepsilon_5$ over land will also affect the accuracy of the coefficients n_i and m_i . By assuming an error $\Delta\varepsilon_4$ and $\Delta\varepsilon_5$ of 0.005 on the emissivities ε_4 and ε_5 and running simulations, we found a total error from 2% to 14% over ocean and from 4% to 21% over land.
- c. Equation (16)** is an approximation, and its uncertainty has been discussed above (from 0.5% to 3.5% RMS).
- d. Transmittance** errors in Channel 3 derives from the uncertainty and the computation of the water vapor and the other atmospheric gases. The accuracy of the formula used to compute the transmittance in Channel 3 [Eqs. (25) and (26)] is about 2%. The water vapor amount is deduced from

$T_4^m - T_5^m$ with an accuracy assumed to be 0.5 g/cm^2 over sea and 0.8 g/cm^2 over land (see above), which generates relative errors of about 5% and 7.5% RMS on the reflectance ρ_3 .

- e. The solar irradiance** E_3 is assumed to be known with an accuracy of 2%, which means 2% in the computation of the reflectance ρ_3 .
- f. Aerosols** may increase the signal in Channel 3 but will decrease the signal in Channels 4 and 5 by the transmittance effect. Assuming an atmosphere with maritime aerosol, the comparison to an aerosol free case gives an error $\Delta\rho_3/\rho_3$ of 30% RMS for $\rho_3=0.02$ and 8% RMS for $\rho_3=0.20$. Over land, the continental type models of aerosols predicts a very low value of the optical thickness, but simulations show that, for very low surface reflectances and for a solar zenith angle of more than 60° , the relative error can reach 10% RMS. For a solar zenith angle of 30° the error decreases to 3%. These errors do not take desert aerosols into account which are spectrally persistent.

Finally, the overall accuracy of the retrieved reflectance in Channel 3 (including the whole range of solar zenith angles) is about 10% for the largest reflectance and about 40% for the lowest.

Table 5a. Coefficients Used for the Computations of the Water Vapor Transmittance in Channel 3 for NOAA 9 and NOAA 11 [Eq. (25)]

	<i>a</i>	<i>b</i>	<i>c</i>
NOAA 9	3.0116	1.289	0.036436
NOAA 11	2.9778	1.2793	0.037785

Table 5b. Coefficients Used for the Computations of the Transmittance of the Other Gases in Channel 3 for NOAA 9 and NOAA 11 [Eq. (26)]

	<i>a</i>	<i>b</i>	<i>c</i>
NOAA 9	0.987	-0.0360	-0.00149
NOAA 11	0.986	-0.0364	-0.00152

TEST OF THE APPROACH

Over Ocean

We tested the formula with five AVHRR scenes over the Pacific Ocean between 1985 and 1990. First we computed images of the reflectance in Channel 3; then we compared them with theoretical computations of sun glint using the Cox and Munk (1954) parametrization that includes an anisotropic distribution of wave slopes. Except for desert aerosols, the effect of aerosols is low in Channel 3 and the driving parameters in determining the reflectance in Channel 3 are the wind speed and its direction. Figure 7 shows the surface reflectance over one sunglint area retrieved using Eq. (17). With the Cox and Munk's model we first defined the wind speed using

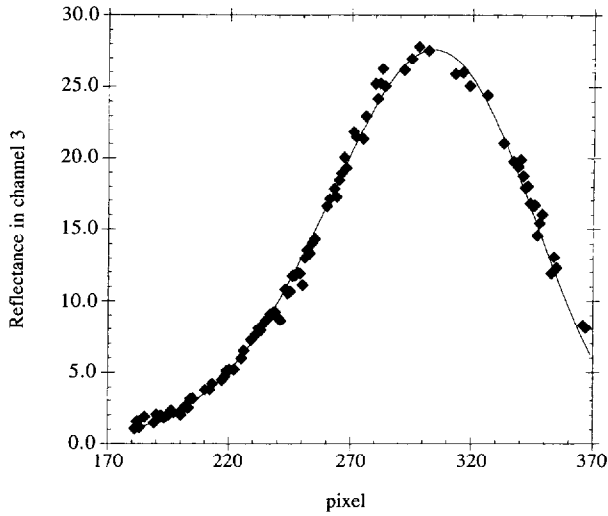


Figure 7. Surface reflectance retrieved in Channel 3 over sunglint. Also reported, comparisons with theoretical computations for a wind speed of 6 m/s and wind direction of 70°.

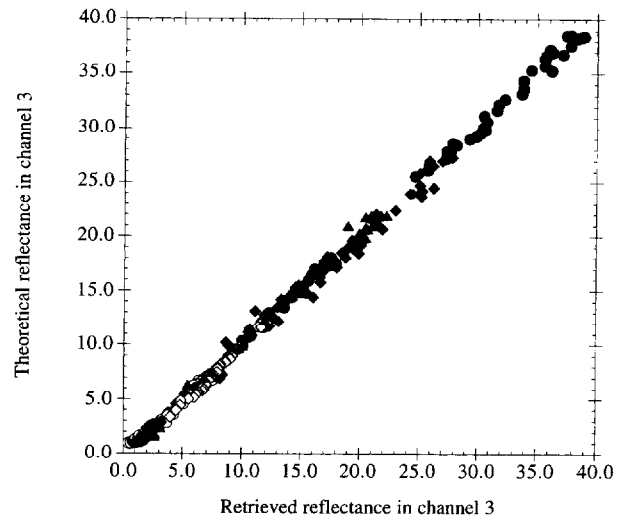


Figure 9. Comparisons for five scenes acquired over sunglint between theoretical (Cox and Munk model) and retrieved reflectance in Channel 3 [Eqs. (9) and (19)].

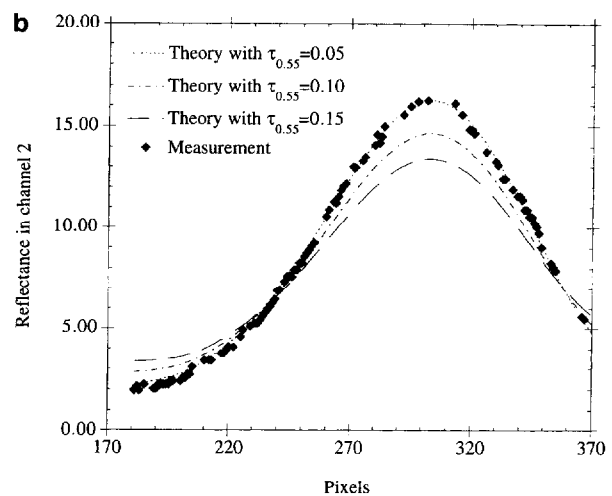
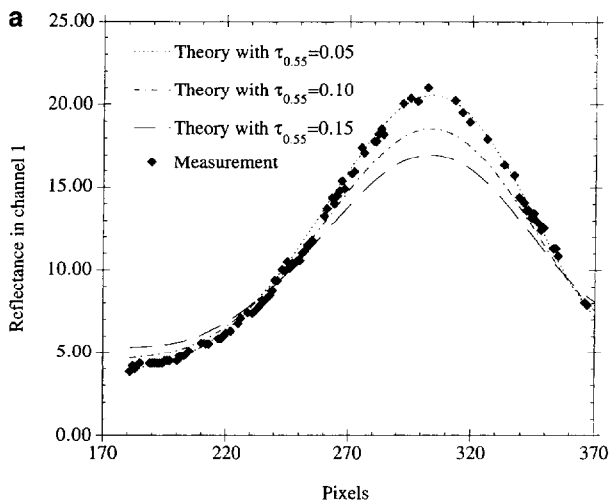
the superior part of the sunglint (highest reflectances), and then defined the direction of the wind using the whole sunglint. For the example shown in Figure 7, we found a speed of 6 m/s and a direction (or azimuth) of about 70°, which is expected in the northern Pacific around 40° of latitude. This shows we have a consistent shape of the sunglint.

To further validate the approach, we computed the signal in Channels 1 and 2 assuming a wind speed of 6 m/s, an azimuth of 70°, and three aerosol optical thicknesses (0.05, 0.10, and 0.15 at 0.55 μm). The aerosol model used is maritime (a good assumption in the middle of the Pacific Ocean), and the ozone content is given by TOMS. As shown in Figures 8a and 8b, results for

an optical thickness of 0.05 fit the measurements in the Channels 1 and 2 with good agreement.

To meet other conditions, we performed the same procedure with the four other scenes. Figure 9 gives the results of the surface reflectance in Channel 3 using the speed and the direction of the wind deduced by the process described above. Figure 10 summarizes the retrieved reflectances in Channels 1 and 2 assuming a constant optical thickness for each transect (one by scene) using the characteristics of the wind defined from Channel 3. The good agreement between the computations and the measurements suggests accurate retrieval of reflectance in Channel 3 and water vapor from T_4 and T_5 . It also suggests a method to retrieve aerosol optical thickness over the sunglint.

Figure 8. (a) Retrieval of the aerosol optical thickness from Channel 1 assuming the speed and the direction of the wind deduced from Channel 3. (b) Same as Figure 8a but from Channel 2.



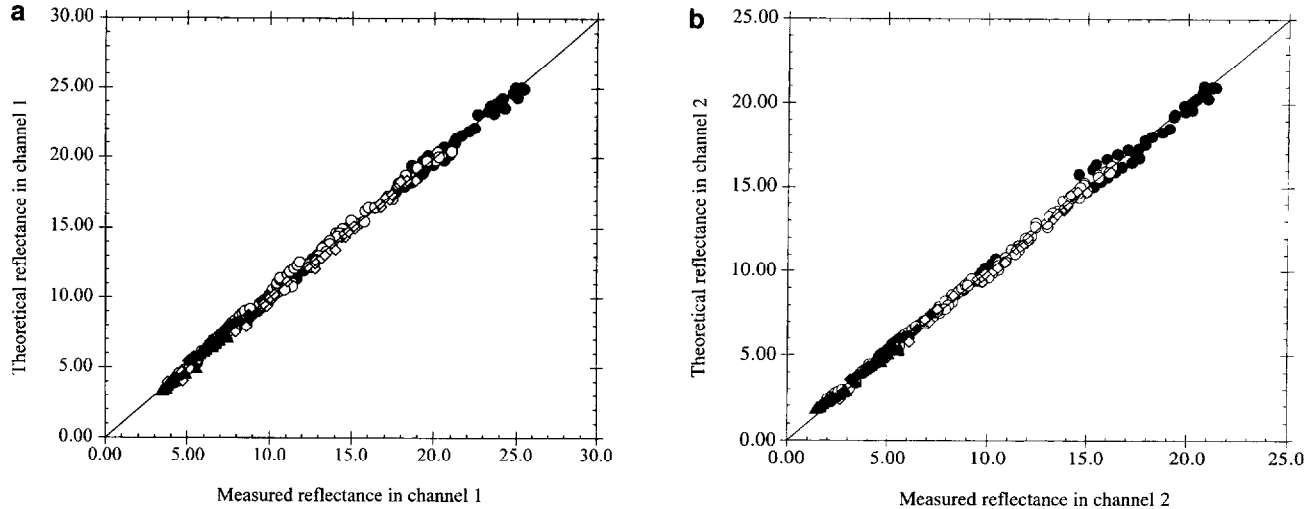
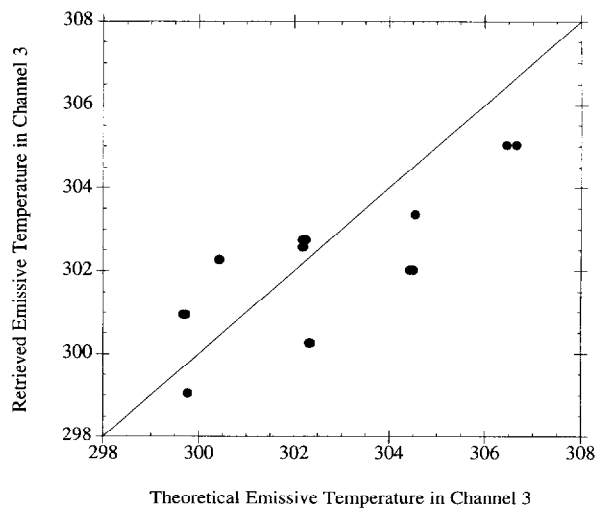


Figure 10. (a) Comparisons for five scenes acquired over sunglint between measured and computed reflectances in Channel 1 assuming retrieved aerosol optical thickness and wind speed (see Figs. 7 and 8a). (b) Same as Figure 10a but for Channel 2.

Over Land

The formula to compute the emissive temperature in Channel 3 with Eq. (19) $T_3^e(\epsilon_3=1)$ has been tested assuming an emissivity in Channels 4 and 5 derived from the NDVI [Eq. (18)] and using the FIFE-87 data set (Sellers et al., 1992). Unfortunately, we do not have in this data set surface reflectance measurements at 3.75 μm . So, we deduced $T_3^e(\epsilon_3=1)$ by simulations from MODTRAN2 using all AVHRR data, atmospheric radiosoundings, surface, and air temperature measurements. Figure 11 shows the comparison between the emissive temperature retrieved using Eq. (19) and the emissive temperature simulated using MODTRAN2 for the clearest days with

Figure 11. Retrieved emissive temperatures in Channel 3 compared to the theoretical ones using the FIFE-87 data set.



radiosoundings. We found for the seven days a mean difference of about 1.75°K.

For further validation, one could simply examine the relationship between Channels 3 and 1. We must see if the correlation between Channels 3 and 1 improves when one uses the reflectance in Channel 3 in lieu of the total radiance.

As pointed out by Kaufman and Remer (1994): “Parallel processes affect the reflectance in Channel 1 (0.67 μm) and Channel 3 (3.75 μm). The presence of vegetation decreases the reflectivity in the visible channels due to chlorophyll absorption and in the mid-IR channels due to absorption by liquid water associated with the plant. Wet soil has a lower reflectance in the visible channels due to light trapping capability, and in 3.75 μm channels due to liquid water absorption. Surface roughness, shadows and inclinations decrease the reflectance across the whole solar spectrum.”

Using the FIFE-87 data set, we compared the surface reflectances in Channels 1 and 3 during the June–September 1987 period. The surface reflectances of Channel 1 were computed for TOA signal using 6S (Verote et al., 1995) and using atmospheric characteristics given by the FIFE data set. Reflectances in Channel 3 were computed using the method described in the present article. A comparison between surface reflectances in Channels 1 and 3 is given Figure 12a for one specific automatic station (station ID 1563) for each satellite overpassing. We used 3×3 AVHRR pixels around the station. In order to be sure that measurements from the automatic station were representative of the local area, a threshold has been performed on the data set selecting a standard deviation less than 50% of the mean value inside the 3×3 pixels. Thus, less than 15% of the days (for this station) has been removed from the data set.

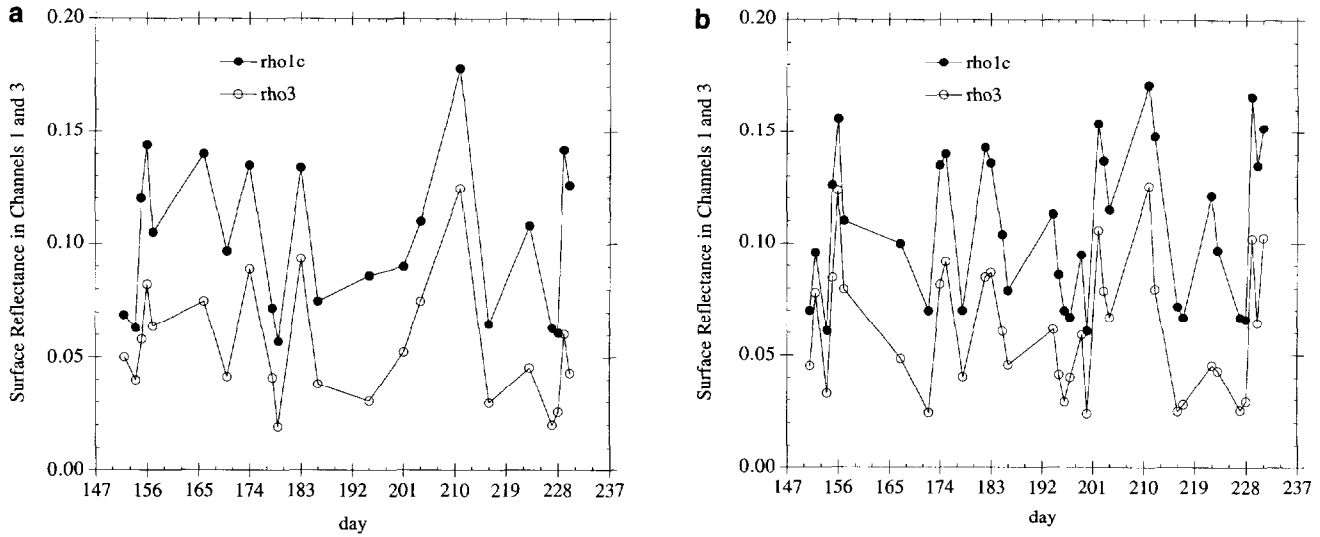


Figure 12. (a) Comparison between the surface reflectance in Channel 1 and the surface reflectance in Channel 3 using the FIFE-87 data set (station ID 1563). (b) Same as Figure 12a but for the whole FIFE-87 site.

We also show the same comparison (Fig. 12b), but using all the cloud-free pixels of the whole FIFE site (101×101 pixels AVHRR-LAC maximum). In both cases, one can observe a good correlation between Channels 1 and 3 which is temporally consistent.

In Figure 13, we show a direct comparison for the whole FIFE site of the reflectance in Channel 1 with either the raw radiance in Channel 3 or the reflectance in Channel 3. There is a very substantial increase in the

correlation when using the reflectance in Channel 3 (from 0.2 to 0.9). Despite the uncertainties inherent to the procedure we adopted, quantitative use of the derived reflectance at 3.75 μm appears possible.

CONCLUSION

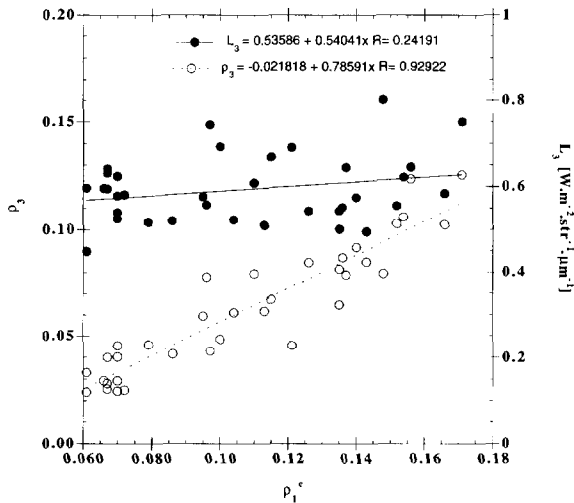
This article has presented a formula for computation of the reflectance in AVHRR Channel 3. The formulation takes into account emissivity, emitted radiation, and atmospheric transmission and only uses AVHRR channels to simplify operational implementation in a processing stream. Sets of coefficients are given for land and ocean and instruments on board the NOAA 9 and 11 satellites. The approach is sufficiently general to be applied to other sensors with similar spectral characteristics.

An error budget is computed and accuracy in derivation of reflectance is found to be of the order of 40% at low reflectance (0.02) and 10% at high reflectance (0.20).

Tentative validation is presented for both ocean and land cases showing a very good agreement for ocean cases. Over land, validation is more difficult due to the absence of direct measurement of Channel 3 reflectance. However, by comparing multiday surface reflectance in Channels 1 and 3, we are able to confirm the correlation between the two channels that are affected by parallel physical processes.

Future work should focus on more validation and application of the reflectance of Channel 3. The formula we have developed should enable some quantitative use of the reflectance at 3.75 μm despite the error inherent to the inversion procedure.

Figure 13. Comparison of the radiance observed in Channel 3 ($W m^{-2} sr^{-1} \mu m^{-1}$) and the reflectance in Channel 3 [deduced from Eq. (16)] with the reflectance observed in Channel 1 corrected for atmospheric effect using 6S. The data corresponds to the whole FIFE site (cf. Fig. 14b).



REFERENCES

- Becker, F., and Li, Z. L. (1990), Towards a local split window method over land surfaces. *Int. J. Remote Sens.* 3:369–393.
- Becker, F., Nerry, F., Ramanantsizehena, P., and Stoll, M. P. (1986), Mesures d'émissivité angulaire par réflexion dans l'infrarouge thermique—implications pour la télédétection. *Int. J. Remote Sens.* 7:1751–1762.
- Berk, A., Berstein, L. S., and Robertson, D. C. (1989), MODTRAN: A Moderate Resolution Model for Lowtran 7, GLTR-89-0122.
- Cox, C., and Munk, W. (1954), Measurement of the Roughness of the Sea Surface from photographs of the Sun's glitter. *J. Opt. Soc. Am.* 44(11):838–850.
- Dalu, G. (1986), Satellite remote sensing of atmospheric water vapor. *Int. J. Remote Sens.* 7(9):1089–1097.
- Daughtry, C. S. T., Gallo, K. P., and Bauer, M. E. (1983), Spectral estimates of solar radiation intercepted by corn canopies. *Agron. J.* 75:527–531.
- Dozier, J. (1981), A method for satellite identification of surface temperature fields of subpixel resolution. *Remote Sens. Environ.* 11:221–229.
- Eck, T. F., and Holben, B. N. (1994), AVHRR split window temperature differences and total precipitable water over land surfaces. *Int. J. Remote Sens.* 15(3):567–582.
- Justice, C. O., Townshend, J. R. G., Holben, B. N., and Tucker, C. J. (1985), Analysis of the phenology of global vegetation using meteorological satellite data. *Int. J. Remote Sens.* 6(8):1271–1318.
- Justice, C. O., Eck, T. F., Tanré, D. and Holben, B. N. (1991), The effect of water vapour on the normalized difference vegetation index derived for the Sahelian region from NOAA AVHRR data. *Int. J. Remote Sens.* 12(6):1165–1187.
- Kaufman, Y. J., and Remer, L. A. (1994), Detection of forests using mid-IR reflectance: an application for aerosol studies. *IEEE Trans. Geosci. Remote Sens.* 32:672–683.
- Kerr, Y. H., Lagouarde, J. P., and Imbernon, J. (1992), Accurate land surface temperature retrieval from AVHRR data with use of an improved split window algorithm. *Remote Sens. Environ.* 41:197–209.
- Kidwell, K. B. (1991), *NOAA Polar Orbiter Data User's Guide*, NOAA/NCDC/SDSD, National Climatic Data Center, Washington, DC.
- Malingreau, J. P., Tucker, C. J., and Laporte, N. (1989), AVHRR for monitoring global tropical deforestation. *Int. J. Remote Sens.* 10:855–867.
- Masuda, K., Takashima, T., and Takayama, Y. (1988), Emissivity of pure and sea waters for the model sea surface in the infrared window regions. *Remote Sens. Environ.* 24:313–329.
- Matson, M., and Dozier, J. (1981), Identification of subresolution high temperature sources using a thermal IR sensor. *Photogramm. Eng. Remote Sens.* 47:1311–1318.
- McMillin, L. M. (1971), A method of determining surface temperature from measurements of spectral radiance at two wavelengths, Ph.D. dissertation, Iowa State University, Ames.
- McMillin, L. M. (1975), Estimation of sea surface temperature from two infrared window measurements with different absorption. *J. Geophys. Res.* 80:5113–5117.
- Nerry, F., Labed, J., and Stoll, M. P. (1988), Emissivity signatures in the thermal IR band for remote sensing: calibration procedure and method of measurement. *Appl. Opt.* 27(4):758–764.
- Ottlé, C., and Vidal-Madjar, D. (1992), Estimation of land surface temperature with NOAA9 data. *Remote Sens. Environ.* 40:27–41.
- Prabhakara, C., Dalu, G., and Kunde, V. G. (1974), Estimation of sea surface temperature from remote sensing in the 11- to 13- μm window region. *J. Geophys. Res.* 79(33):5039–5044.
- Rao, N. C. R., Stowe, L. L., and McClain, E. P. (1989), Remote sensing of aerosols over the ocean using AVHRR data. Theory, practice and applications. *Int. J. Remote Sens.* 10(4–5):743–749.
- Roger, J. C., Vermote, E., and El Saleous, N. (1994), Atmospheric correction of MAS data during SCAR-A experiment. In *The European Symposium on Satellite Remote Sensing in Atmospheric Sensing and Modeling*, Rome, 29–30 September, Proc. SPIE Vol. 2311, pp. 83–89.
- Salisbury, J. W., and D'Aria, D. M. (1992), Emissivity of terrestrial materials in the 8–14 μm atmospheric window. *Remote Sens. Environ.* 42:83–106.
- Schluessel, P. (1989), Satellite derived low level atmospheric water vapor content from synergy of AVHRR with HIRS. *Int. J. Remote Sens.* 10(4–5):705–721.
- Schubert, S. D., Pjaendtner, J., and Rood, R. (1993), An assimilated data set for Earth science applications. *Bull. Am. Meteorol. Soc.* 74:2331–2342.
- Seguin, B., Fisher, A., Kerdules, H., et al. (1992), Suivi agroclimatique des cultures en France à partir des données NOAA, METEOSAT et SPOT. In *2nd Conference on Remote Sensing Applied to Agricultural Statistics*, Belgirate, Italy, 26–27 November 1991, pp. 339–342.
- Sellers, P. J., Hall, F. H., Asrar, G., et al. (1992), An overview of the First International Satellite Land Surface Climatology Project (ISLSCP) Field Experiment (FIFE). *J. Geophys. Res.* 97(D17):18,345–18,371.
- Setzer, A. W., and Pereira, M. C. (1991), Amazon biomass burning in 1987 and their tropospheric emissions. *Ambio.* 20:19–22.
- Takashima, T., and Takayama, Y. (1981), Emissivity and reflectance of the model sea surface for the use of AVHRR data of NOAA satellites. *Pap. Meteorol. Geophys.* 32(4):267–274.
- Tucker, C. J., Holben, B. N., Elgin, J. H., and McMurtry, J. E. (1981), Remote sensing of total dry matter accumulation in winter wheat. *Remote Sens. Environ.* 11:171–189.
- Tucker, C. J., Vanpraet, C. L., Boerwinkel, E., and Gaston, A. (1983), Satellite remote sensing of total dry accumulation in the Senegalese Sahel. *Remote Sens. Environ.* 13:461–474.
- Tucker, C. J., Vanpraet, C. L., Sharman, M. J., and Van Ittersum, G. (1985), Satellite remote sensing of total herbaceous biomass production in the Senegalese Sahel: 1980–1984. *Remote Sens. Environ.* 17:233–249.
- Van de Griend, A. A., and Owe, M. (1993), On the relationship between thermal emissivity and the normalized difference vegetation index for natural surfaces. *Int. J. Remote Sens.* 14(6):1119–1131.
- Vermote, E., El Saleous, N., Holben, B. N., Kaufman, Y. J., and Tucker, C. J. (1992), Global aerosol climatology over tropical belt using AVHRR data. In *IRS'92 Current Problems in Atmospheric Radiation* (S. Keavallik and O. Kärner, Eds.), Kluwer Academic Publisher's Group, Dordrecht, the Netherlands, pp. 191–194.

Vermote, E., El Saleous, N., and Roger, J. C. (1994), Operational atmospheric correction of AVHRR visible and near-infrared data. In *The European Symposium on Satellite Remote Sensing, in Atmospheric Sensing and Modeling*, 29–30 September, Rome, Proc. SPIE Vol. 2311, pp. 141–149.

Vermote, E. F., Tanré, D., Deuzé, J. L., et al. (1995), Second

simulation of the satellite signal in the solar spectrum: an overview. *IEEE Trans. Geosci. Remote Sens.*

Weinreb, M. P., Hamilton, G., Brown, S., and Koczor, R. J. (1990), Nonlinearity corrections in calibration of Advanced Very High Resolution Radiometer infrared channels. *J. Geophys. Res.* 95(C5):7381–7388.